

REAL-TIME TOTAL FOCUSING METHOD FOR ULTRASONIC IMAGING OF MULTILAYERED OBJECT

Wenkai Cui, Kaihuai Qin*

Department of Computer Science and Technology, Tsinghua University, Beijing, China

ABSTRACT

In imaging of multilayered object, total focusing method (TFM) combined with ray-tracing appeals to numerous researchers because of its superior image quality. But lots of iterative computation to calculate the incident points greatly increases its processing time. Based on line scan-conversion algorithm and Snell's principle, this paper proposes an efficient method to calculate the incident point. By dividing the image area into multiple regions, the time-consuming iterative calculation of point of incidence (POI) is eliminated. After introducing this method into TFM, the time complexity of Region-Division (RD) TFM is reduced by one order of magnitude. The simulation experiments validate that the imaging speed of RD-TFM is improved dozens of times compared to traditional TFM with ray-tracing. Besides, RD-TFM applies to multilayered objects with both planar and non-planar interface.

Index Terms— Ultrasonic phased array, Multi-layered object, Total focusing method, Full matrix capture

1. INTRODUCTION

In non-destructive testing (NDT), the tested specimen with irregular surface profile needs to be immersed in water to be closely coupled with the phased array. Hence, the imaging of multilayered object has a wider range of application compared to homogeneous object. Considering that refraction occurs when sound wave propagates through the interface between different media, the point of incidence (POI) at the interface need to be located to get the accurate propagation path. Among all methods to calculate POI, the iterative method is applicable to arbitrary surface profile, which is in dominate position [1] [2].

Recently, the total focusing method (TFM) is favored by plenty of researchers [3] [4] because it is capable of utilizing the maximum information acquired from the phased array and outperforms any other post-processing algorithm [5]. Therefore, TFM combined with ray-tracing is one of the most common used method for imaging of multilayered objects [6] [7]. However, both TFM and the iterative computation of POI require lots of computing power, which restricts its

application in real-time inspection. Lots of effort have been devoted to increasing its performance. For every (element, pixel) pair, precalculating and recording the time of flight from element to pixel can avoid plenty of repeated computation [8] [9]. Because of the high parallelizability of TFM, performing TFM in parallel over GPU is proved to be extremely effective, but this strategy requires more processing resource and appropriate distribution [10] [11]. Sparse array is another way to improve the performance of TFM, but greatly reducing the number of elements may affect the precision of the result image [12]. Compared to time-domain TFM, frequency-domain TFM [13] [14] [15] [16] is able to remove the iterative computation of POI, which will bring a tremendous performance improvement, but most algorithms do not apply to irregular multilayered objects. Auto-focused virtual source imaging (AVSI) can also avoid the iterative calculation by creating virtual sources at the interface [17] [18], but the inspection process is different from traditional full matrix capture (FMC) and the coverage area becomes smaller.

Inside of locating the incident for every (element, pixel) pair, the motion trajectory method presets the incident point, then acquire the pixel on the propagation path, but this method only deals with the situation that the transmitter and the receiver are identical [19]. Based on the identical principle, this paper divides the image area into multiple regions and the incident point in each region is already known, which avoids the interpolation between adjacent refractive vectors in motion trajectory method.

The rest of this paper is organized as follows: section 2 gives a detailed description of RD-TFM and compares its time complexity to preprocessing TFM with ray-tracing. Two immersion testing experiments are simulated to prove the effectiveness of RD-TFM in section 3. The last section gives a summary.

2. REGION-DIVISION TFM

In total focusing method combined with ray-tracing, the pixel value $p(x, z)$ is expressed as follows:

$$I[p(x, z)] = \sum_{t=0}^{N-1} \sum_{r=0}^{N-1} S_{t,r} (T_t(x, z) + T_r(x, z)) \quad (1)$$

Where N is the number of elements in phased array, and $T_t(x, z)$ (or $T_r(x, z)$) represents the time of flight between the

* Corresponding author

element E_t (or E_r) and $p(x, z)$. In order to avoid repeated computation, $T_t(x, z)$ is precalculated and recorded [8]. Based on Fermat's principle, Fig. 1 shows the iterative method to calculate POI: for every point p' at the interface, calculate the transmission time along the propagation path $E_t \rightarrow p' \rightarrow p(x, z)$ and select the point P_i with minimum time of flight as the incident point.

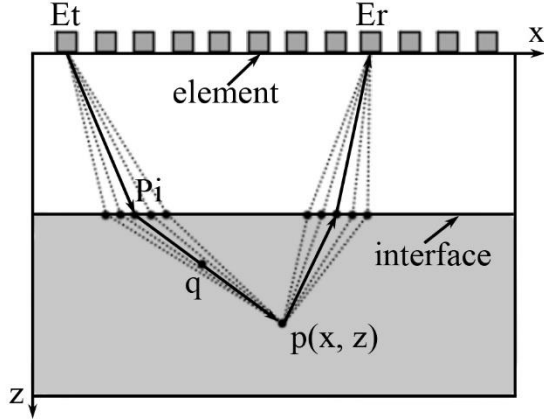


Fig. 1. Iterative method to calculate the point of incidence (POI). Every point q on refractive vector $\vec{P}_i p$ shares the same incident point P_i .

We can see that pixels on the same propagation path share the identical POI [19]: P_i is the incident point between E_t and p in Fig. 1, for every point q on line $P_i p$, its corresponding POI is also P_i . Therefore, for every point P_i at the interface, the incident vector is $\vec{E}_t P_i$ and the refractive vector can be calculated based on Snell's law. After introducing the line scan-conversion algorithm to obtain the coordinates of points on the refractive vector, multiple incident points is acquired at the same time.

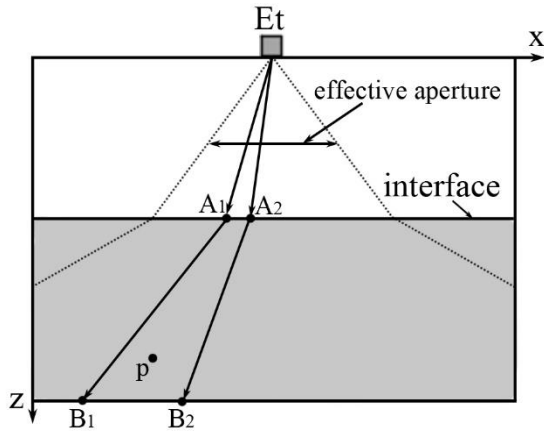


Fig. 2. Region division algorithm to calculate POI. The corresponding POI of every point p within region $A_1 A_2 B_2 B_1$ is either A_1 or A_2 and the one with minimum transmission time is chosen as the incident point.

There exists points which are not passed by refractive vectors. As is shown in Fig. 2, A_1, A_2 are adjacent pixels at the interface and $\vec{A}_1 B_1, \vec{A}_2 B_2$ are the corresponding refractive vectors. For every pixel p within the quadrilateral region $A_1 A_2 B_2 B_1$, the transmission time $T_t(p)$ is still unknown. When the incident point move from A_1 to A_2 , the refractive vector changes from $\vec{A}_1 B_1$ to $\vec{A}_2 B_2$. Therefore, the POI between E_t and p is either A_1 or A_2 , we select the one with minimum transmission time as its POI.

There exists a situation that one point is in multiple regions. a, b and a', b' are adjacent pixels at the interface in Fig. 3. Point q is in both regions: $abcd$ and $a'b'd'c'$. Hence, there are four candidate POIs: a, b, a', b' . The transmission times along all these paths are calculated: $E_t \rightarrow a(b, a', b') \rightarrow p$ and $T_t(p)$ is assigned the minimum value according to Fermat's principle.

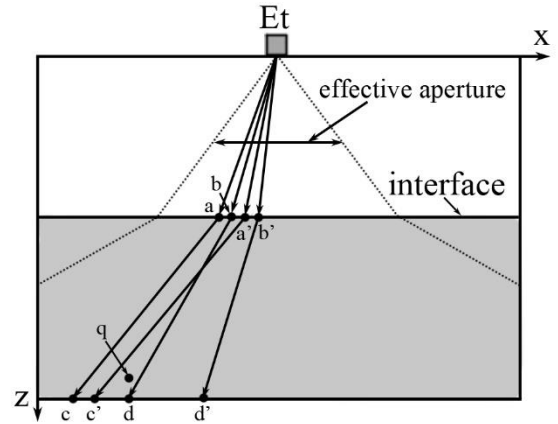


Fig. 3. Special situation: one point q in multiple regions. For every candidate POI, select the one with minimum transmission time as the incident point.

Based on the above analysis, suppose the size of result image is $X_L \cdot Z_L$ and the entire RD-TFM is described as follows:

Algorithm 1 RD-TFM

Input: the full matrix $S_{t,r}, E_k(x_k, 0), 0 \leq t, r, k \leq N - 1$.

Output: $I(x, z), 0 \leq x \leq X_L - 1, 0 \leq z \leq Z_L - 1$.

1. Call TFM to generate the image of the first layer and the interface by assuming the tested object is homogeneous.
2. For every phased array element $E_k(x_k, 0), 0 \leq k < N - 1$, perform 3-5 (region division method).
3. For every two incident points $A_1 A_2$ at the interface, perform 4-5.
4. Calculate their corresponding refractive vectors $\vec{A}_1 B_1, \vec{A}_2 B_2$. For every pixel p within the quadrilateral $A_1 A_2 B_2 B_1$, perform 5.
5. Calculate the transmission times along both propagation paths $E_k \rightarrow A_1 \rightarrow p$ and $E_k \rightarrow A_2 \rightarrow p$, then compare both values to existing value $T_k(p)$, assign $T_k(p)$ the minimum value.

6. Use Eq. (1) to calculate the value of every pixel in the resultant image.

In preprocess TFM combined with ray-tracing, the iterative method with time complexity $O(X_L)$ is called once for each (element, pixel) pair. While in RD-TFM, the POI is chosen between two adjacent points whose time complexity is $O(1)$. Thus, to calculate the transmission time for all (element, pixel) pairs, the total time complexity of preprocessing TFM is $O(N \cdot X_L^2 \cdot Z_L)$ and that of RD-TFM is only $O(N \cdot X_L \cdot Z_L)$. Therefore, the acceleration effect is more obvious when the image size increases.

3. EXPERIMENT

To acquire the full matrix, two immersion testing experiments are simulated by matlab software package k-wave [20]. All post-processing algorithms are running on a PC with Intel® Core™ i5-4210 CPU @ 1.7GHz and 4GB RAM. The range of pixel value in result images is [0, 255].

3.1. Multilayered object with planar surface

The structure of tested object with planar surface is displayed in Fig. 4. The linear phased array contains 50 equally-spaced elements and there are five side drilled holes (SDH) inside the tested object.

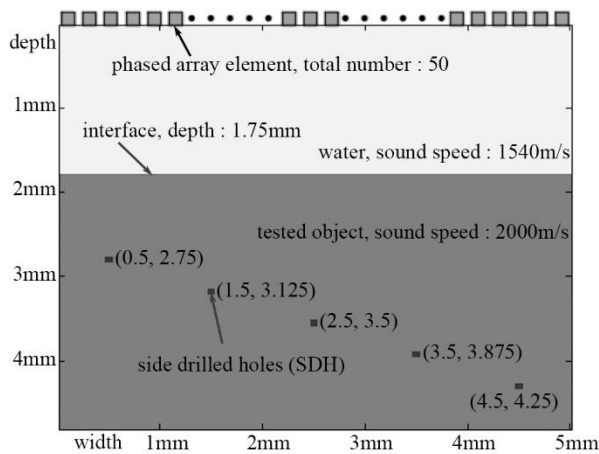


Fig. 4. The structure of tested multilayered object with planar interface. The phased array contains 50 elements and five SDHs are inside the tested object.

The result images of the preprocessing TFM combined with ray-tracing and RD-TFM are shown in Fig. 5(a) and Fig. 5(b), respectively. To facilitate the comparison between Fig. 5(a) and Fig. 5(b), the difference image between both images is calculated and shown in Fig. 5(c). Obviously, both images are exactly the same, but the imaging speed of RD-TFM (2192.35s) is 24 times faster than the conventional TFM method (90.601s).

The maximum amplitudes along the depth direction of both result images are plotted in Fig. 5(d). Considering both

result images are identical, both plots coincide with each other. Each plot contains six peaks and each peak means the pixels at current depth are coherently summed. The first peak corresponding to the interface between different media and the latter five peaks are related to five SDHs, respectively. After comparing the depths of six peaks with real structure of tested object in Fig. 4, both algorithms are capable of locating SDHs precisely.

The speedup ratios under different image sizes are plotted in Fig. 8. Clearly, the acceleration effect of RD-TFM improves as the image size increases.

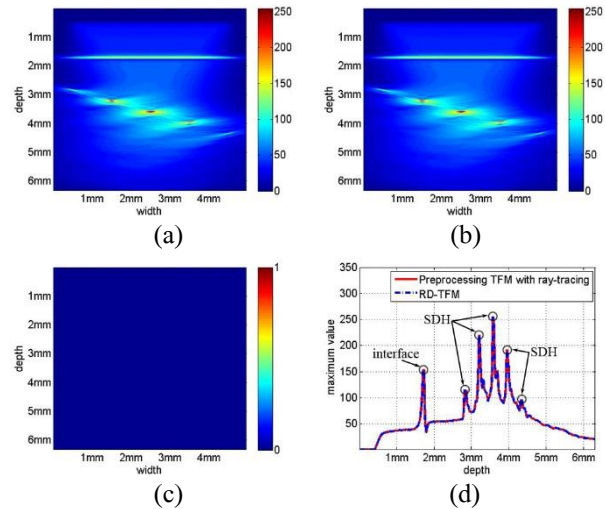


Fig. 5. The result images constructed by (a) Preprocessing TFM with ray-tracing. (b) RD-TFM. (c) Difference image between (a) and (b). (d) Maximum amplitude along the depth direction.

3.2. Multilayered object with non-planar surface

The structure of tested object with irregular surface profile is shown in Fig. 6. The phased array is identical to the one used in the previous experiment.

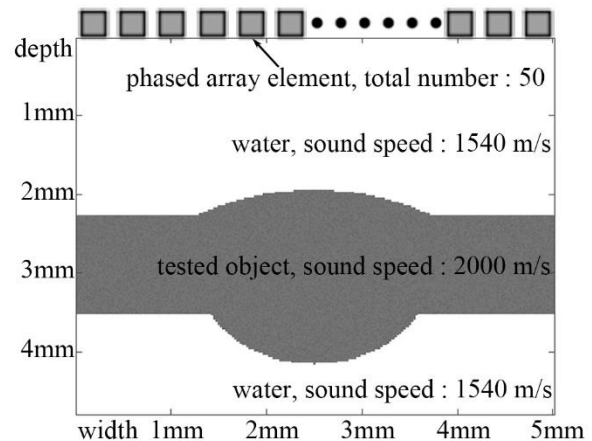


Fig. 6. The structure of tested object with irregular surface profile

Both preprocessing TFM combined with ray-tracing and RD-TFM are used to get the surface profile of the tested object. Fig. 7(a) and Fig. 7(b) display their result images, respectively. To easily compare both images, Fig. 7(a) is selected as the reference and Fig. 7(c) represents the difference image between Fig. 7(a) and Fig. 7(b). The maximum absolute value in Fig. 7(c) is 10 and the average value is 0.0344. Considering the range of pixel value is [0, 255], the slight difference is negligible. To further evaluate the quality of both images, the boundaries of tested objects in Fig. 7(a) and Fig. 7(b) are extracted and displayed in Fig. 7(d). The plotted curve of RD-TFM coincide with that of conventional TFM, which verifies that RD-TFM applies to ultrasonic imaging of irregular multilayered objects. Similarly, the superiority of RD-TFM in performance is also proven judging from Table. 1 and Fig. 8: the processing time of the conventional TFM (2223.08s) is 22 times longer than RD-TFM (99.507s).

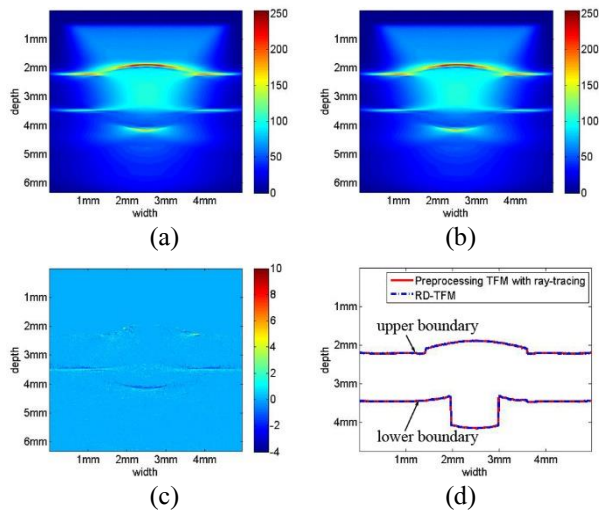


Fig. 7. Result images constructed by (a) Preprocessing TFM with ray-tracing. (b) RD-TFM. (c) Difference image between (a) and (b). (d) The profiles of multilayered object extracted from (a) and (b).

Table 1. The processing times of preprocessing TFM with ray-tracing and RD-TFM under both experiments.

Experiment	Algorithm	Time
Experiment 3.1	Preprocessing TFM	2192.35s
Experiment 3.1	RD-TFM	90.601s
Experiment 3.2	Preprocessing TFM	2223.08s
Experiment 3.2	RD-TFM	99.507s

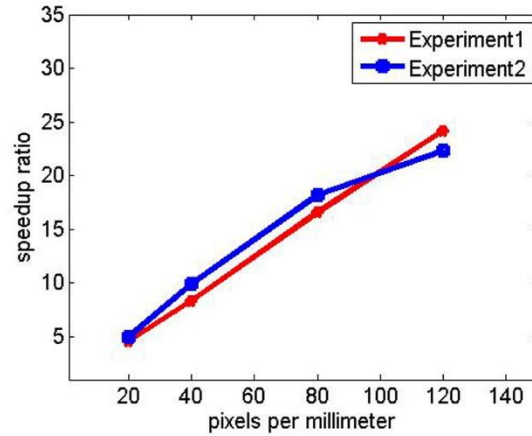


Fig. 8. The speedup ratio of RD-TFM under different image sizes (pixels per millimeter).

4. CONCLUSION

In imaging of multilayered objects, the iterative computation of POI occupies most of the processing time, which has become a performance bottleneck for its application in real-time inspection. This paper proposes a novel method to calculate POI based on region division (RD). The image area is first divided into several regions. For pixels in the same region, its corresponding POI is chosen from only two pixels at the interface, lowering the time complexity by one order of magnitude. Two immersion testing experiments are simulated to validate the efficiency of RD-TFM: one with a planar surface profile and the other with nonplanar surface. Both experiments prove the correctness and efficiency of RD-TFM.

RD-TFM can be combined with other optimization techniques such as GPU to achieve better performance, which will be our future work.

5. REFERENCES

- [1] M. Weston, "Advanced Ultrasonic Digital Imaging and Signal Processing for Applications in the Field of Non-Destructive Testing," 2012.
- [2] J.A. Ogilvy, "An iterative ray tracing model for ultrasonic nondestructive testing," *NDT & E International*, vol. 25, no. 1 pp. 3-10, 1992.
- [3] J. Zhang, T. Barber, Nixon, A., and P. Wilcox, "Investigation into distinguishing between small volumetric and crack-like defects using multi-view total focusing method images," *AIP Conference Proceedings*, vol. 1806, no. 1, pp. 040003, 2017.
- [4] E. Iakovleva, S. Chatillon, P. Bredif, and S. Mahaut, "Multimode TFM imaging with artifacts filtering using CIVA UT forwards models," *AIP Conference Proceedings*, vol. 1581, no. 1, pp. 72-79, 2014.
- [5] C. Holmes, B.W. Drinkwater, and P.D. Wilcox, "Post-processing of the full matrix of ultrasonic transmit-receive array data for non-destructive evaluation," *NDT & E International*, vol. 38, no. 8, pp. 701-711, 2005.
- [6] J.A. Ogilvy, "An iterative ray tracing model for ultrasonic nondestructive testing," *NDT & E International*, vol. 25, no. 1 pp. 3-10, 1992.
- [7] O. Nowers, D. J. Duxbury, and B. W. Drinkwater, "Ultrasonic array imaging through an anisotropic austenitic steel weld using an efficient ray-tracing algorithm," *NDT & E International*, vol. 79, pp. 98-108, 2016.
- [8] M. Njiki, A. Elouardi, S. Bouaziz, O. Casula, and O. Roy, "A real-time implementation of the total focusing method for rapid and precise diagnostic in non destructive evaluation," *Application-Specific Systems, Architectures and Processors (ASAP), 2013 IEEE 24th International Conference on*, pp. 245-248, 2013.
- [9] M. Njiki, A. Elouardi, S. Bouaziz, O. Casula, and O. Roy, "A multi-FPGA architecture-based real-time TFM ultrasound imaging," *Journal of Real-Time Image Processing*, pp. 1-17, 2016.
- [10] M. Sutcliffe, M. Weston, B. Dutton, P. Charlton, and K. Donne, "Real-time full matrix capture for ultrasonic non-destructive testing with acceleration of post-processing through graphic hardware," *NDT & E International*, vol. 51, pp. 16-23, 2012.
- [11] D. Romero-Laorden, J. Villazon-Terrazas, O. Martinez-graullera, A. Ibanez, M. Parrilla, and M.S. Penas, "Analysis of parallel computing strategies to accelerate ultrasound imaging processes," *IEEE Transactions on Parallel and Distributed Systems*, vol. 27, no. 12, pp. 3429-3440, 2016.
- [12] P. Rocca, G. Oliveri, R. J. Mailloux, and A. Massa, "Unconventional phased array architectures and design methodologies—A review," *Proceedings of the IEEE*, vol. 104, no. 3, pp. 544-560, 2016.
- [13] T. Stepinski, "An implementation of synthetic aperture focusing technique in frequency domain," *IEEE transactions on ultrasonics, ferroelectrics, and frequency control*, vol. 54, no. 7, pp. 1399-1408, 2007.
- [14] T. Olofsson, "Phase shift migration for imaging layered objects and objects immersed in water," *IEEE transactions on ultrasonics, ferroelectrics, and frequency control*, vol. 57, no. 11, 2010.
- [15] M. H. Skjelvareid, T. Olofsson, Y. Birkelund, and Y. Larsen, "Synthetic aperture focusing of ultrasonic data from multilayered media using an omega-k algorithm," *IEEE transactions on ultrasonics, ferroelectrics, and frequency control*, vol. 58, no. 5, pp. 1037-1047, 2011.
- [16] H. Wu, J. Chen, K. Yang, and X. Hu, "Ultrasonic array imaging of multilayer structures using full matrix capture and extended phase shift migration," *Measurement Science and Technology*, vol. 27, no. 4, pp. 045401, 2016.
- [17] J. Camacho, and J. F. Cruza, "High resolution autofocused virtual source imaging (AVSI)," *Ultrasonics Symposium (IUS), 2015 IEEE International*, pp. 1-4, 2015.
- [18] J.F. Cruza, and J. Camacho, "Total Focusing Method With Virtual Sources in the Presence of Unknown Geometry Interfaces," *IEEE transactions on ultrasonics, ferroelectrics, and frequency control*, vol. 63, no.10, pp. 1581-1592, 2016.
- [19] C. Yang, K. Qin, and Y. Li, "Real-time ultrasonic imaging for multi-layered objects with synthetic aperture focusing technique," *Instrumentation and Measurement Technology Conference (I2MTC) Proceedings, 2014 IEEE International*, pp. 561-566, 2014.
- [20] B.E. Treeby, and B.T. Cox, "k-Wave: MATLAB toolbox for the simulation and reconstruction of photoacoustic wave fields," *Journal of biomedical optics*, vol. 15, no. 2, pp. 021314-021314, 2010.